Since January 2020 Elsevier has created a COVID-19 resource centre with free information in English and Mandarin on the novel coronavirus COVID-19. The COVID-19 resource centre is hosted on Elsevier Connect, the company's public news and information website.

BASIC SCIENCE

Nanomedicine: Nanotechnology, Biology, and Medicine
34 (2021) 102388

Original Article

nanomedjournal.com

Cerium oxide nanoparticle delivery of microRNA-146a for local treatment of acute lung injury

Stephen M. Niemiec, MD[a,1], Sarah A. Hilton, MD[a,1], Alison Wallbank, BS[b], Mark Azeltine, MS[a], Amanda E. Louiselle, MD[a], Hanan Elajaili, PhD[c], Ayed Allawzi, PhD[c], Junwang Xu, PhD[a], Courtney Mattson, BS[b], Lindel C. Dewberry, MD[a], Junyi Hu, MD[a], Sushant Singh, PhD[d], Tamil S Sakthivel, PhD[d], Sudipta Sea, PhD[d,e], Eva Nozik-Grayck, MD[c], Bradford Smith, PhD[b], Carlos Zgheib, PhD[a], Kenneth W. Liechty, MD[a,*]

[a]*Laboratory for Fetal and Regenerative Biology, Department of Surgery, University of Colorado Denver School of Medicine and Children's Hospital Colorado, Aurora, CO, USA*

[b]*Department of Bioengineering, University of Colorado, Aurora, CO, USA*

[c]*Cardiovascular Pulmonary Research Laboratories and Pediatric Critical Care Medicine, Department of Pediatrics, University of Colorado, Aurora, CO, USA*

[d]*Department of Material Science and Engineering, Advanced Materials Processing and Analysis Center, Nanoscience Technology Center, University of Central Florida, Orlando, FL, USA*

[e]*College of Medicine, UCF Prosthetics Cluster, University of Central Florida, Orlando, FL, USA*

Revised 22 February 2021

Abstract

Acute respiratory distress syndrome (ARDS) is a devastating pulmonary disease with significant in-hospital mortality and is the leading cause of death in COVID-19 patients. Excessive leukocyte recruitment, unregulated inflammation, and resultant fibrosis contribute to poor ARDS outcomes. Nanoparticle technology with cerium oxide nanoparticles (CNP) offers a mechanism by which unstable therapeutics such as the anti-inflammatory microRNA-146a can be locally delivered to the injured lung without systemic uptake. In this study, we evaluated the potential of the radical scavenging CNP conjugated to microRNA-146a (termed CNP-miR146a) in preventing acute lung injury (ALI) following exposure to bleomycin. We have found that intratracheal delivery of CNP-miR146a increases pulmonary levels of miR146a without systemic increases, and prevents ALI by altering leukocyte recruitment, reducing inflammation and oxidative stress, and decreasing collagen deposition, ultimately improving pulmonary biomechanics.

Key words: Acute lung injury; Acute respiratory distress syndrome; Cerium oxide nanoparticles (CNP); microRNA-146a (miR146a)

Acute Respiratory Distress Syndrome (ARDS) is a highly morbid pulmonary disease characterized by hypoxic respiratory failure and long-term sequelae of pulmonary fibrosis and respiratory dysfunction.[1–4] The disease carries an in-hospital mortality of nearly 40% and has a rising incidence due to coronavirus-associated ARDS. Multiple etiologies increase the risk of ARDS development, including trauma, pneumonia, and sepsis, which share a common pathogenesis of unrestrained inflammation and oxidative stress. Unfortunately, current management of acute lung injury (ALI) that progresses to ARDS is limited to supportive care with mechanical ventilation, highlighting the need for therapeutic innovation.

Conflicts of Interest and Source of Funding: This work was supported by a Gates Center Grubstake Award for the work presented in this publication. Additionally, E.N., C.Z., and K.L. report financial interest in Ceria Therapeutics.

* Corresponding author at: Barbara Davis Center for Childhood Diabetes, Aurora, CO.
E-mail address: ken.liechty@cuanschutz.edu. (K.W. Liechty).

[1] Denotes co-first author.

https://doi.org/10.1016/j.nano.2021.102388

Please cite this article as: Niemiec SM, et al, Cerium oxide nanoparticle delivery of microRNA-146a for local treatment of acute lung injury. *Nanomedicine: NBM* 2021;34:102388, https://doi.org/10.1016/j.nano.2021.102388

Intratracheal drug delivery systems offer the benefit of direct therapeutic delivery to the diseased site while avoiding potential degradation seen in intravenous and gastro-intestinal delivery.[5] This permits high dose drug delivery while minimizing systemic response, as has been seen in effective gene delivery in models of endobronchial cancer.[6] Effective pulmonary delivery has to overcome natural barriers in the lung, such as surfactant, mucus, and ciliated endothelium. Nanotechnology offers a potential vector for local pulmonary delivery.

Cerium oxide nanoparticle (CNP), or nanoceria, is an earth-based nanomedicine that is a promising carrier molecule for local treatment of acute lung injury. CNP has radical scavenging properties due to its multivalent +3 and +4 oxidation states,[7–13] and a recent review has highlighted the potential of CNP in treatment of ALI and coronavirus-associated ARDS.[14] Briefly, along with its antioxidant potential, CNP has been shown to inhibit the nuclear factor kappa-light-chain-enhancer of activated B cells (NFκB) inflammatory pathway, which activates pro-inflammatory cytokines interleukin (IL)-6, IL-8, and tissue necrosis factor alpha (TNFα). These inflammatory pathways have been shown to be key mediators in the pathogenesis of ALI and ARDS.[9,15,16] Furthermore, CNP inhibits transforming growth factor beta (TGF-β), which is upregulated in the early phases of ALI and a key component in the pathogenesis of pulmonary fibrosis associated with ARDS.[17,18]

Nanotechnology further offers a stable delivery system for otherwise unstable therapeutics, such as microRNAs (miR, miRNA). miRNAs have rapid pharmacokinetics given their small size and negative charge, and are degraded by ubiquitous tissue nucleases, resulting in overall instability as an unmodified therapeutic.[19,20] CNP, when conjugated to miRNA, may protect the miRNA from oxidative damage while neutralizing its negative charge to promote cellular uptake.[21–24] miR146a is an anti-inflammatory miRNA that inhibits tumor necrosis factor 6 (TRAF6) and interleukin-1 receptor associated kinase 1 (IRAK1), promotors of NFκB.[25] Downstream, miR146a therefore plays an intrinsic role in downregulating pro-inflammatory mediators IL-6, IL-8, and TNFα.[25] miR146a has been shown to be modestly upregulated in ALI to downregulate inflammatory pathways and correct injury, and upregulation of miR146a has shown promise in downregulating pro-inflammatory pathways in models of ALI.[26,27] We have conjugated the anti-inflammatory miR146a to CNP, termed CNP-miR146a, to synergistically target the oxidative stress and inflammation seen in acute lung injury and ARDS.

We hypothesize that intratracheal delivery of CNP-miR146a will result in local increases in miR146a levels without systemic exposure to the treatment. To evaluate the therapeutic effects on preventing lung injury with local delivery of CNP-miR146a, we will utilize a well-established murine model of ALI/ARDS with toxic exposure to bleomycin. This injury results in a significant inflammatory and oxidative stress response that later progresses to fibrosis, as is seen in ARDS. We hypothesize that intratracheal administration of CNP-miR146a after bleomycin-induced acute lung injury reduces the inflammatory infiltrate, decreases pro-inflammatory cytokine levels, and lowers oxidative stress, thereby preventing alveolar damage and improving pulmonary function.

Methods

Nanoparticle development and miR146a conjugation

Cerium oxide nanoparticles were synthesized and oxidized, as previously described.[28,29] Briefly, CNP was synthesize using a precipitation method. $Ce(NO)_3$, $6H_2O$ was dissolved in deionized in water and oxidized from cerium (III) ions to cerium (IV) oxide with the use of excess hydrogen peroxide. The solution is then maintained at a pH below 3.5 to maintain a suspension of ceria nanoparticle. Upon oxidation, the crystalline nanoparticles precipitate and were isolated by centrifugation at 8000 ×*g*. Five mM of nanoceria suspension was diluted in pure water to obtain a final nanoceria concentration of 10 μM. Conjugation of CNP to miR146a was performed by utilizing the activated form of 1,1-carbonyldiimidazole (CDI) to couple the amino group of miR146a to the CNP hydroxyl group. The conjugated CNP-miR146a was diluted to 100 ng/50 μL in phosphate buffered saline (PBS) for intratracheal dosing. An MTT assay for CNP-miR146a toxicity was performed in vitro, and a full description of MTT assay methods can be found in Supporting Information (SI).

Animal model

Eight- to 10-week-old male mice (C57BL/6, strain no. 000642, Jackson Laboratory) were used after allowing the animals to acclimate to our 1600 m altitude for 1 week. Care of the animals was in accordance with the guidelines defined in the NIH Guide for the Care and Use of Laboratory Animals. Animal protocols were approved by the Institutional Animal Care and Use Committee (IACUC) at University of Colorado Denver–Anschutz Medical Campus (License #84-R-0059). Each measurement was taken from distinct samples.

Pulmonary and systemic distribution of CNP-miR146a in uninjured mice

Uninjured mice were given intratracheal delivery of 100 ng CNP-miR146a in 50 μL PBS (n = 5 for all time points). Animals were euthanized at 0, 3, 12, 24, 72, and 168 h after treatment for whole lung harvest and blood collection. Mice harvested at 0, 12, and 24 h had liver, kidneys, heart, and spleen harvested. Organ tissue was processed for total RNA extraction by homogenizing in Qiazol (Qiagen) per manufacturer's instructions. Isolated RNA samples were diluted to 5 ng/μL by serial dilution and converted to U6 and miR146a cDNA (Applied Biosystems RT kit), which was amplified by reverse transcriptase amplification using the BioRad CFX-9600 thermal cycler. Real-time quantitative polymerase chain reaction (RT-qPCR) was performed for miR146a with the U6 housekeeper gene used for normalization. PCR analysis was performed in triplicate with the average of each triplicate used for normalization. Additional methods for comparative pathology of control and CNP-miR146a treated mice are included in SI.

Prior to lung harvest in the above mice, blood was collected via right atrial puncture in an EDTA lined syringe and tube. Blood samples were centrifuged at 3000 rpm for 15 min and the plasma layer was isolated. A second centrifugation at 3000 rpm for 5 min was performed and the collected plasma was stored for processing. Lung and plasma from mice sacrificed at 0, 3, 12, 24,

72, and 168 h were processed for inductively coupled plasma mass spectrometry (ICP-MS) for determination of cerium concentration. Briefly, samples were digested for 72 h in 1 mL 70% nitric acid at 40 °C. Following digestion, samples were diluted with deionized water while ensuring nitric acid concentration of 5%. Following dilution, samples were syringe filtered using a 0.22 μm membrane filter prior to analysis.

Bleomycin injury and treatment model

Bleomycin is a well-accepted model of acute lung injury that produces a short-term inflammatory response followed by long-term pulmonary fibrosis, a similar pattern seen in severe cases of ALI/ARDS.[30–32] Mice were injured with five units/kg bleomycin or an equivalent weight-based volume of PBS (Control group). The bleomycin-injured mice were further divided into four treatment groups. One group received no treatment (Bleo group). The remaining group received a concurrent treatment at time of injury of 100 ng CNP-miR146a (Bleo + CNP-miR146a group), 100 ng CNP alone (Bleo + CNP alone), or 20 ng miR146a alone (Bleo + miR146a), where CNP and miR146a are the component doses of the conjugate treatment, CNP-miR146a, which were determined by ultraviolet vis spectrophotometry and hydrodynamic size measurement.

Electron paramagnetic resonance (EPR) spectrometry for reactive oxygen species (ROS) detection

Lung tissue harvested 7 days following injury (n = 5, 10, 7, 7, 11 for control, bleo, bleo + CNP, bleo + miR146a, bleo + CNP-miR146a) was homogenized in sucrose buffer in a 1:6 ratio of lung weight to buffer volume (0.25 M sucrose, 10 mM TRIS–HCl, 1 mM EDTA, pH = 7.4). 60 μL of lung homogenate for each sample was mixed with 140 μL of Krebs-HEPES buffer (KHB) consisting of 100 μM DTPA and 0.2 mM CMH. A blank sample of 200 μL KHB was used for background signal subtraction. The samples were incubated for 1 h at 37 °C and 150 μL samples were loaded in PTFE tubing with rubber seal stoppers.[33] ROS production was measured by EPR spectrometry using the superoxide selective spin probe 1-hydroxy-3-methoxycarbonyl-2, 2, 5, 5-tetramethylpyrrolidine (CMH). The Bruker EMX nano X-band spectrometer was used at 77 K with Bruker liquid nitrogen Finger Dewar to detect ROS as CM•. EPR acquisition parameters were: microwave frequency = 9.65 GHz; center field = 3438 G; modulation amplitude = 4.0 G; sweep width = 150 G; microwave power = 0.316 mW; total number of scans = 10; sweep time = 60 s; and time constant = 1.28 ms. CM• nitroxide radical concentration was obtained by double integration followed by Spin count (Bruker).

Quantitative real-time PCR (RT-qPCR)

Lung tissue used for RT-PCR was collected 3 days, 7 days, and 14 days following bleomycin-induced lung injury (n = 7 for all treatment groups, n = 14 at 7 days for the Bleo group). Harvested lung tissue was homogenized and processed for RT-qPCR as described above. Normalization was attained using the housekeeper genes GAPDH for mRNA. Expression analysis of pro-inflammatory TNFα, IL-6, and IL-8, and pro-fibrotic TGFβ-1, Col1α2, and Col3α1 was performed. All samples were examined in triplicate and the average of each triplicate was used for statistical analysis of each sample.

Immunohistochemistry

Lung tissue was harvested at time of euthanasia 14 days after injury. The left lung was inflated with melted agarose solution with care to not overinflate the lung. Once inflated, the lung was removed and placed in 4% Paraformaldehyde (PFA) in 10 mL sterile PBS incubated on ice. The lung was kept in PFA at room temperature for 24 h, then dehydrated in 70% EtOH, and embedded in paraffin prior to sectioning at 4 μm. Slides were stained with Mason's trichrome, which stains collagen fibers blue. Twenty high-power fields at 400× total magnification were randomly imaged for each sample by an independent researcher. A second researcher then used an automated algorithm on NIS Elements–Advanced Research imaging software to quantify collagen deposition by area of blue staining. The average area per HPF was averaged for each sample prior to comparative analysis (n = 7 for all treatment groups).

Slides used for immunohistochemistry were deparaffinized and placed in a citrate buffer (pH 6.0). Biocare Medical's Decloaker was used to retrieve the heat-induced epitope and slides were stained with Leica's Bond Rx instrument. Primary CD45 antibodies at 1:50 solutions (BD Biosciences) were applied to the slides, and the slides were developed with a Vectastain Elite ABC kit (Vector Laboratories). Slides were analyzed as described above for the number of CD45-positive cells per high-power field by evaluating twenty random high-power fields at 400× total magnification and averaging counts for each sample with the use of two independent researchers (n = 7 for all treatment groups).

Pulmonary function testing

Fourteen days after lung injury a cohort of mice were invasively ventilated to measure lung function (n = 12, 8, 6, 5, 11 for control, bleomycin, bleomycin + CNP, bleomycin + miR146a, bleomycin + CNP-miR146a groups). Mice were anesthetized with 100 mg/kg ketamine, 16 mg/kg xylazine, and 3 mg/kg acepromazine via intraperitoneal (IP) injection. Following tracheostomy with an 18-gauge metal cannula, the mice were ventilated with a computer-controlled rodent ventilator (SCIREQ flexiVent). Respiratory drive was suppressed with 0.8 mg/kg IP pancuronium bromide and the electrocardiogram was used to monitor anesthesia. A baseline ventilation with a tidal volume 10 ml/kg at 200 breaths per minute and PEEP = 3 cmH_20 was applied for 10 min to allow the mice to stabilize on the ventilator. Recruitment maneuvers (RM) consisting of a 3-s ramp to 30 cmH2O and a 3-s breath hold were applied at 2-min intervals during the stabilization period. Lung function assessments included an RM followed immediately by a stepwise 16-s pressure-volume (PV) loop with a maximum pressure of 30 cmH_2O. The PV loop data were used to calculate the quasi-static compliance at 5 cmH_2O on the expiratory limb, PV loop hysteresis area, and the delivered volume which we refer to as the inspiratory capacity. In addition, an RM was applied and immediately followed by four 3-s multi-frequency forced oscillations (3 ml/kg, 13 mutually prime frequencies from 1 to 20.5 Hz) at 10-s intervals to measure pulmonary system impedance. The impedance data

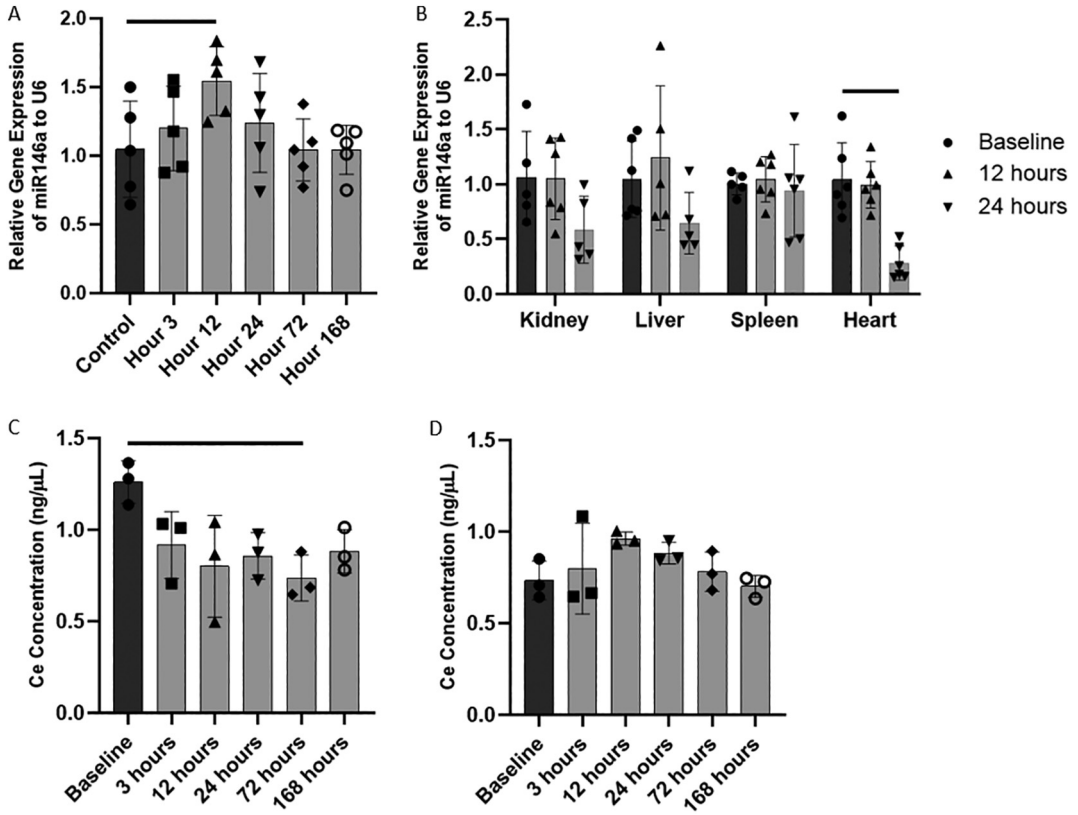

Figure 1. Local delivery of CNP-miR146a to the lung.**(A)** Relative levels of miR146a normalized to U6 in the lung at various timpoints after IT delivery. IT delivery of CNP-miR146a significantly increases miR146a levels at 12 h, but normalizes to control levels by 24 h after delivery. **(B)** IT delivery of CNP-miR146a results in no significant increase in miR146a levels in kidney, liver, heart, and spleen tissue. **(C)** CNP concentration decreases to below baseline at 72 h after IT administration of CNP-miR146a. **(D)** IT CNP-miR146 does not increase plasma CNP concentration over time. Bars indicate statistical significance with $P < 0.05$. Mean and standard deviation values are shown.

were fit to the constant phase model[34] to determine elastance, tissue damping, and central airway resistance.

Statistical analyses

Comparison of quantitative data between multiple treatment groups was performed using one-way ANOVA with a two-sided level of significance $\alpha = 0.05$. The mean of each treatment group was compared to the means of the control and bleomycin treatment groups.

Results

CNP and CNP-miR146a cause no cell toxicity

MTT assay of cell viability for fibroblasts exposed to 24 h of CNP or CNP-miR146a demonstrated >95% cell viability for both treatment groups (Figure S1).

Increases in miR146a is limited to the lung after intratracheal administration of CNP-miR146a

The relative levels of miR146a in lung, kidney, liver, spleen, and heart tissue after intratracheal administration of CNP-miR146a were performed using RT-qPCR. Twelve hours after intratracheal delivery, miR146a levels were significantly higher in the lung than at baseline (Figure 1, *A*, $P = 0.0459$; 95% CI: [0.01, 0.98]), and returned to baseline by 24 h following administration. miR146a levels within the lung remained at baseline up to 168 h after intratracheal delivery. There was no significant increase in miR146a levels in kidney, liver, heart, or spleen (Figure 1, *B*).

Ce concentration levels remain stable in the lung with no systemic increase

Cerium concentration was measured using ICP-MS for lung and plasma levels over time after IT administration of 100 ng/50 μL CNP-miR146a in uninjured mice. Ce concentration was significantly lower in the lung 72 h after administration compared to baseline levels (Figure 1, *C*, $P = 0.0234$), however there was no change in systemic plasma levels over the course of 168 h. The maximum average plasma concentration was 0.9623 ng/μL 12 h after CNP-miR146a administration, but this was not significantly different from baseline (Figure 1, *D*, $P = 0.2859$). Comparative pathology analysis of mice treated with saline or CNP-miR146a is included in SI.

CNP and CNP-miR146a lower inflammatory cell infiltrate

Histologic evidence of inflammatory cell infiltration was evaluated using CD45+ staining in lung tissue harvested 14 days following bleomycin injury (Figure 2, *A-E*). Bleomycin-injured mice demonstrated significantly higher CD45+ cells per high-

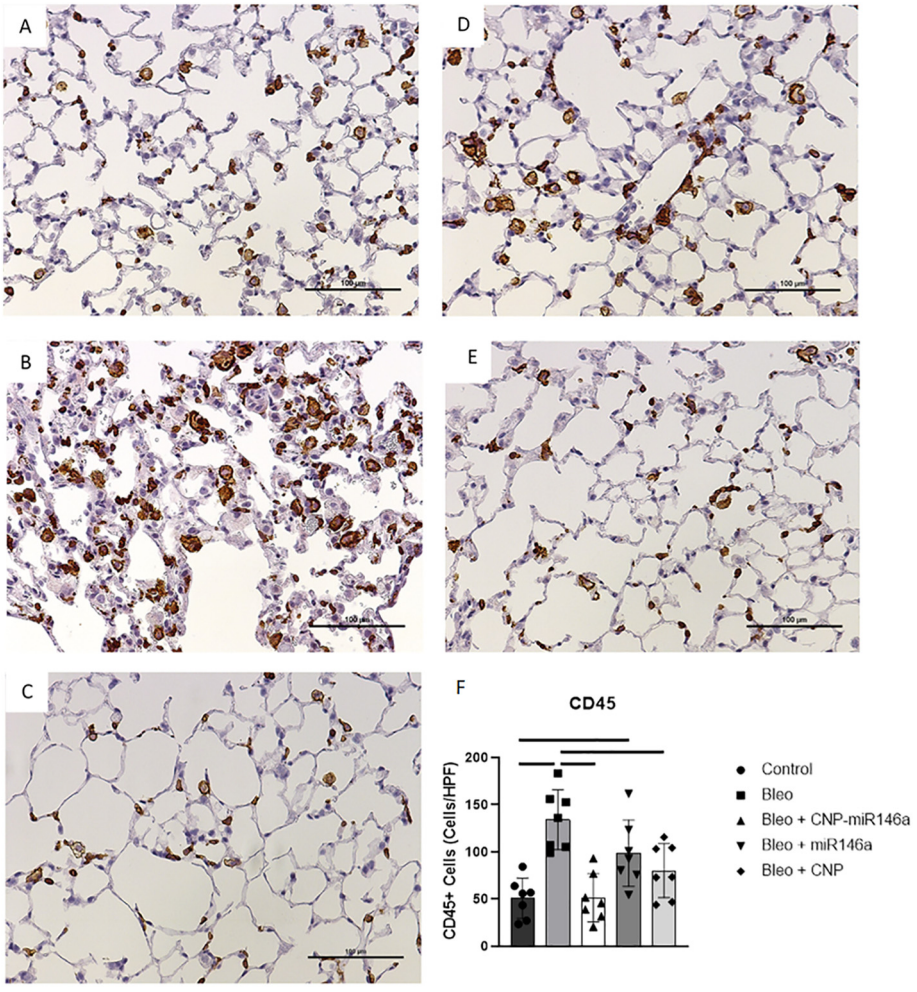

Figure 2. Reduction of inflammatory cell infiltrate with CNP-miR146a.**(A-E)** CD45+ stained 4 μm slides at 200× power 14 days following bleomycin instillation. **(A)** Control, **(B)** bleomycin, **(C)** bleomycin + CNP-miR146a, **(D)** bleomycin + miR146a, **(E)** bleomycin + CNP. **(F)** CD45+ cells present in lung samples were significantly higher in bleomycin-injured lungs, and treatment with CNP-miR146a and CNP alone significantly reduced inflammatory cell infiltrate number. Mean and standard deviation values from $n = 7$ samples per group are shown.

powered field (HPF) compared to controls ($P < 0.0001$; 95% CI: [38.77, 128.3]). Preventative treatment with CNP-miR146a significantly decreased the number of CD45+ cells present (Figure 2, *F*, $P < 0.0001$; 95% CI: [38.23, 127.7]), as did CNP alone (Figure 2, *F*, $P = 0.0115$; 95% CI: [9.472, 98.96]).

ROS production in the lung is lowered by CNP, miR146a, and CNP-miR146a

The concentration of CM• following oxidation of 1-hydroxy-3-methoxycarbonyl-2, 2, 5, 5-tetramethylpyrrolidine (CMH), a superoxide selective nitroxide probe, was measured in lungs harvested at 14 days following injury using electron paramagnetic resonance (EPR) spectrometry. Bleomycin-injured lungs had higher nitroxide concentrations of 169 μM than control concentrations of 126 μM ($P = 0.0239$, 95% CI: [−82.05, −4.161]). All treatment groups had lower nitroxide concentrations than bleomycin-injured lungs as depicted in Figure 3 ($P < 0.0001$, $F = 11.12$, $R^2 = 0.5596$).

Pro-inflammatory gene expression

To evaluate the effects of CNP-miR146a on pro-inflammatory gene expression, real-time quantitative polymerase chain reaction (RT-qPCR) was performed on right lung digests. Figure 4 depicts the relative gene expression of IL-6, IL-8, and TNFα at 3-, 7-, and 14-days post injury. Three days after injury, there was a significant increase in IL-6, IL-8, and TNFα gene expression in bleomycin-injured mice compared to uninjured controls (Figure 4, *A-C*, $P < 0.0001$, 95% CI: [3.132, 8.044]; $P = 0.0104$, 95% CI: [0.4816, 3.987]; $P = 0.0258$, 95% CI: [0.1932, 3.453]). Preventative treatment with CNP-miR146a significantly lowered IL-6 gene expression compared to untreated, bleomycin-injured mice 3 days following injury ($P = 0.0002$, 95% CI: [−7.202, −2.290]). To test the individual components of the conjugate treatment, CNP-miR146a, treatment with equivalent doses of miR-146a mimic and CNP alone was performed. Treatment with miR146a and CNP showed similar decreases in IL-6 expression 3 days after injury ($P = 0.007$, 95% CI: [−6.680, −1.767]; $P = 0.007$, 95% CI: [−6.698, −1.785]).

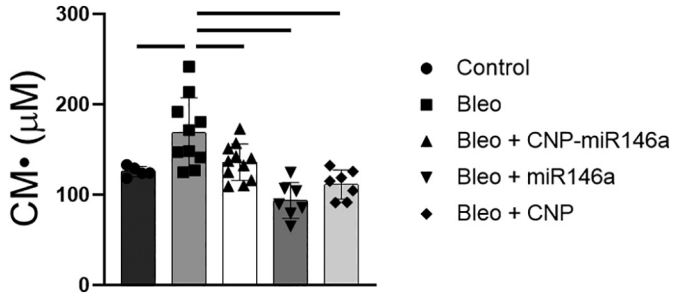

Figure 3. ROS levels 14 days following bleomycin injury measured by EPR.CM• nitroxide reactive oxygen species concentration was significantly higher in bleomycin-injured lungs compared to controls ($P = 0.0239$), with all treatments normalizing nitroxide concentration to control levels, and reduced to significantly lower levels when compared to untreated bleomycin-injured lungs ($P < 0.05$). Bars indicate statistical significance with $P < 0.05$. Mean and standard deviation values are shown from $n = 5, 10, 11, 7, 7$ for control, bleomycin, bleomycin + CNPmiR146a, bleomycin + CNP, bleomycin + miR146a samples per group.

Seven days after bleomycin injury, there was a significant upregulation in IL-6 and IL-8 compared to controls (Figure 4, *E-G*, $P < 0.0001$, 95% CI: [2.96, 8.668]; $P = 0.0002$, 95% CI: [1.244, 4.824]). CNP-miR146a treatment lowered expression of IL-8 and TNFα compared to untreated, injured lungs ($P = 0.0297$, 95% CI: [−3.312, −0.1221]; $P = 0.0124$, 95% CI: [−2.384, −0.2115]). MiR-146a mimic treatment lowered IL-8 and TNFα gene expression compared to bleomycin-injured lungs that did not receive treatment ($P = 0.0495$, 95% CI: [−3.361, −0.0024]; $P = 0.0339$, 95% CI: [−2.234, −0.0615]). Two weeks following bleomycin injury, expression of IL-6, IL-8, and TNFα returned to control levels in bleomycin-injured lungs with no difference between treated and untreated groups (Figure 4, *I-K*).

Pulmonary fibrosis is attenuated by CNP-miR146a

RT-qPCR was performed on pro-fibrotic genes TGFβ-1, Col1α2, and Col3α1. TGFβ-1 expression was significantly elevated three days after injury in the bleomycin group compared to controls ($P = 0.0464$, 95% CI: [0.01, 1.17]), but was significantly lowered by one-treatment with CNP-miR146a (Figure 4, *D*, $P = 0.0064$, 95% CI: [−1.13, −0.20]). TGFβ-1 gene expression normalized to control levels in all groups at day 7 and day 14 (Figure 4, *H*, *L*). CNP-miR146a lowered Col1α2 relative gene expression 7 days following injury (Figure S2, $P = 0.0034$, 95% CI: [−0.8492, −0.1525]). Col1α2 was upregulated 7 days after injury in bleomycin-injured lungs compared to controls ($P = 0.0009$, 95% CI: [0.2382, 1.054]), with gene expression significantly lower in CNP-treated and miR146a-treated lungs compared to untreated, bleomycin-injured lungs ($P < 0.0001$, 95% CI: [−1.226, −0.4408]; $P < 0.0001$, 95% CI: [−1.217, −0.4321]). There was no significant difference in Col1α2 gene expression among groups at 14 days following injury or in Col3α1 at 7 or 14 days after injury.

Histologic evaluation of inflation-fixed lung tissue was performed on tissue harvested 14 days following injury to assess overall architectural change and the degree of fibrosis. 4 μm sections were trichrome stained and area of collagen per HPF was quantified for each treatment group 14 days following bleomycin injury using NIS-Elements–Advanced Research computer software. Bleomycin injury increased collagen levels compared to controls per HPF ($P = 0.0354$, 95% CI: [33.24, 1313]). There was a significant reduction in area of collagen per HPF with CNP-miR146a treatment ($P = 0.0125$, 95% CI: [−1408, −127.7]) compared to bleomycin-injured mice (Figure 5, *F*).

Pulmonary function

Pulmonary function was measured during invasive mechanical ventilation 14 days after bleomycin injury (Figure 6). Quasi-static pressure-volume loop analysis shows that, compared to uninjured controls, the bleomycin-injured mice had significantly lower compliance at 5 cmH20 on the expiratory limb ($P < 0.0001$, 95% CI: [−0.03787, −0.01721]) and decreased inspiratory capacity ($P < 0.0001$, 95% CI: [−0.303, −0.942]), while hysteresis was not significantly changed. Multi-frequency forced oscillation impedance measurements recorded at PEEP = 0 cmH_2O and fit to the constant phase model show that bleomycin increased pulmonary system elastance ($P = 0.0005$, 95% CI: [7.619, 35.30]) and tissue resistance ($P = 0.0003$, 95% CI: [1.186, 5.507]) while central airway resistance was unaffected. Preventative treatment with CNP-miR146a restored pulmonary compliance, elastance, tissue resistance, and inspiratory capacity to control levels. When compared to untreated, bleomycin-injured lung, CNP-miR146a treatment significantly improved compliance ($P = 0.0107$, 95% CI: [0.00222, 0.0229]), inspiratory capacity ($P = 0.018$, 95% CI: [0.0154, 0.228]), elastance ($P = 0.0324$, 95% CI: [−27.99, −0.869]), and tissue resistance ($P = 0.0362$, 95% CI: [−3.868, − -0.0967]).

Discussion

In this experiment, we have shown that intratracheal administration of CNP-miR146a localizes to the lung and prevents bleomycin-induced lung injury through downregulation of inflammation and oxidative stress. CNP-miR146a is the conjugation of multivalent CNP to the anti-inflammatory miR146a. The conjugate size on average is 190 nm, which has previously been described in detail with Transmission Electron Microscopy (TEM).[35] CNP has previously been shown to be taken up by endocytosis, and cellular toxicity in various cell lines, including a human lung cancer cell line A549, which showed no toxicity after 24 h of CNP exposure at concentrations

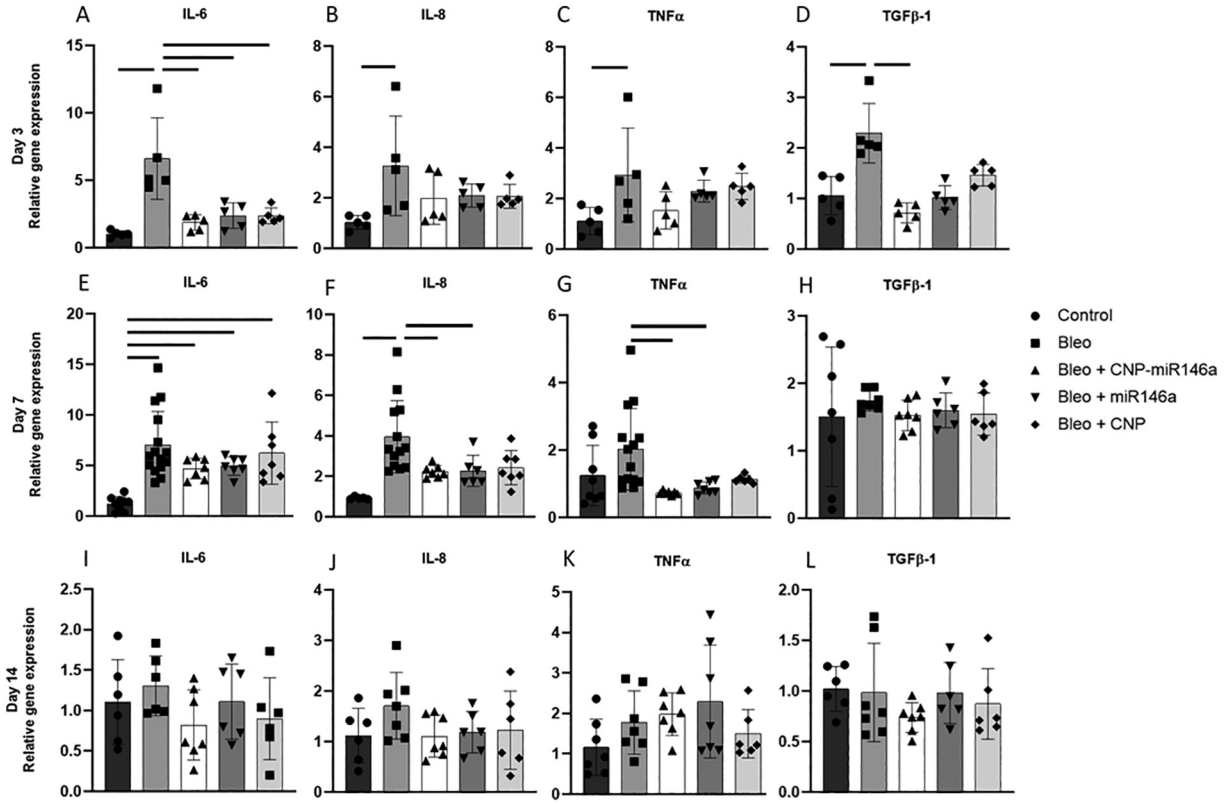

Figure 4. Pro-inflammatory and pro-fibrotic gene expression is decreased after CNP-miR146a treatment.Relative gene expression of pro-inflammatory markers 3- **(A-D)**, 7- **(E-H)**, and 14-days **(I-L)** after bleomycin injury with comparison to GAPDH housekeeping gene expression. Bleomycin injury significantly raised IL-6, IL-8, TNFα, and TGFβ-1 gene expression compared to controls. IL-6 and TGFβ-1 relative gene expression was significantly reduced with CNP-miR146a 3 days following injury, while IL-8 and TNFα gene expression was significantly lowered with CNP-miR146a treatment 7 days following injury. CNP and miR146a mimetic also lowered IL-6 gene expression at day 3, while miR146a mimetic also lowered IL-8 and TNFα gene expression 7 days following injury. Bars indicate statistical significance with $P < 0.05$. Mean and standard deviation for $n = 7$ samples are shown.

up to 2000 μg/mL, 1000 times the concentration of our tested IT dose, consistent with our data demonstrating no cellular toxicity with CNP or CNP-miR146a (Figure S1).[36,37] The 100 ng dose chosen for this study was based on our previous work with CNP-miR146a in diabetic wounds.[38] A single IT application of 100 ng/50 μL CNP-miR146a successfully prevented bleomycin-induced lung dysfunction by down regulating inflammatory gene signaling, lowering oxidative stress, and preventing significant fibrotic changes. We plan to test optimal dosing in a future study where treatments are administered days after onset of injury, a more clinically relevant model.

CNP conjugation to miR146a neutralizes the negative charge on the anti-inflammatory miRNA, allowing for stable uptake of miR146a in the lung at twelve hours after intratracheal administration without significant changes in pulmonary cerium concentration. The level of miR146a in the lung normalizes by 24 h after intratracheal delivery, which would allow for repeat dosing in a clinical setting should there be ongoing injury. Importantly, there is no significant increase in miR146a in major organ systems outside of the lung or cerium within the plasma. Additionally, four weeks after therapy, there was no histopathologic injury difference between PBS and CNP-miR146a therapy in the brain, heart, lung, spleen, kidney, jejunum, or ileum (Table S1). The lack of systemic increase in cerium and miR146a and lack of systemic toxicity highlight the benefit of local administration directly to the site of injury.

Bleomycin-induced lung injury results in a robust inflammatory response with increased inflammatory cell recruitment. Leukocytes, identified histologically using CD45+ staining, play a critical role in the development of ALI. Alveolar macrophages, for instance, play a critical role in both the development of ALI and its resolution as it transitions from a pro-inflammatory activation state to a pro-resolving/anti-inflammatory phenotype.[39,40] Nanoceria has been shown to inhibit NFκB, which lowers important chemokines involved in leukocyte recruitment, such as IL-6 and IL-8.[16] We see a robust infiltration of leukocytes on histologic analysis of lung tissue 14 days following injury, and treatment with CNP-miR146a reduced this leukocyte infiltrate, as did CNP alone (Figure 2).

Leukocytes play an important role in free radical production, and excess oxidative stress is intrinsic to the pathogenesis of ALI and ARDS, with higher levels of ROS promoting the release of pro-inflammatory cytokines.[39] CNP, miR146a, and CNP-miR146a all lowered CM• nitroxide production to control levels (Figure 3). The reduction in ROS by CNP could be secondary to its multivalency, as has been seen in other disease models,[41] as well as its anti-inflammatory properties and reduction in leukocyte recruitment. We have previously shown that CNP-

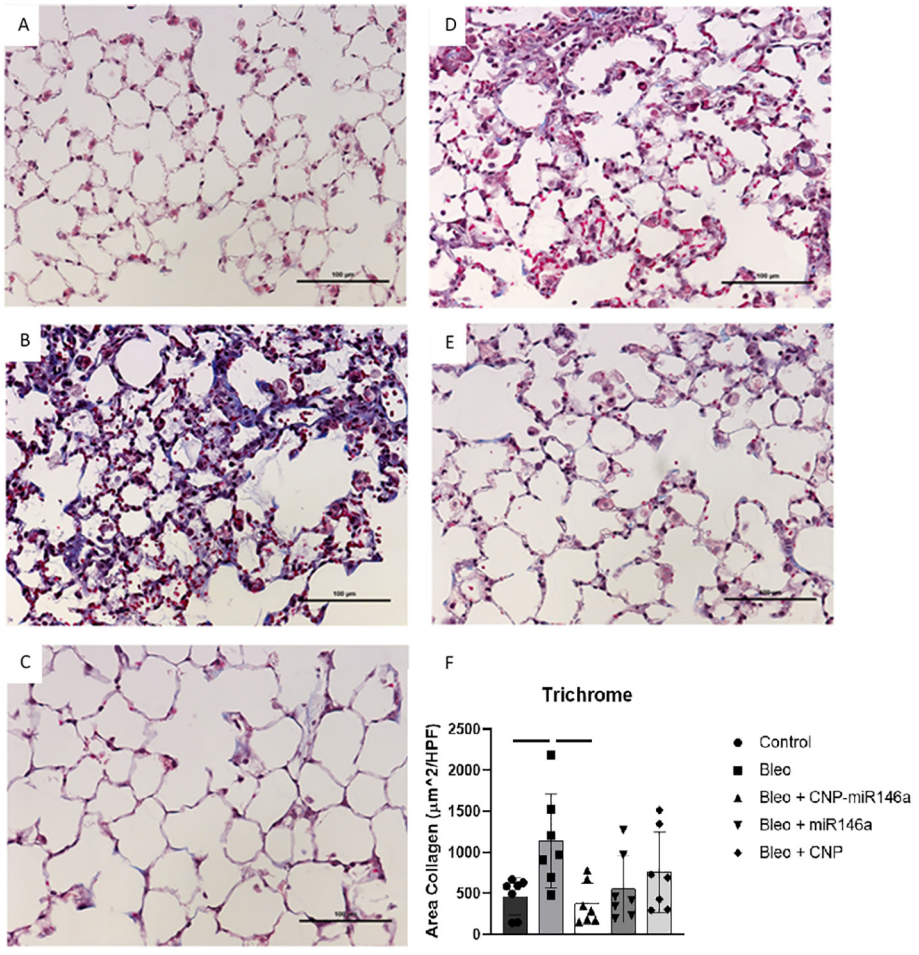

Figure 5. Collagen levels 14 days after bleomycin injury are decreased following CNP-miR146a treatment.Trichrome staining at 200× power **(A)** control, **(B)** bleomycin, **(C)** bleomycin + CNP-miR146a, **(D)** bleomycin + miR146a, and **(E)** bleomycin + CNP lungs. **(F)** Trichrome quantification of collagen deposition averaged over 20 random high-powered fields (HPF) at 400× power. Bleomycin injury resulted in altered histologic structure and increased collagen deposition in bleomycin-injured lungs compared to controls. CNP-miR146a treatment and miR146a treatment significantly reduced collagen deposition per HPF compared to bleomycin-injured lungs. Bars indicate statistical significance with $P < 0.05$. Mean and standard deviation for $n = 7$ samples are shown.

miR146a targets the NF-κB pro-inflammatory pathway by inhibiting TRAF6 and IRAK1.[38] Downregulation of these pathways by miR146a has been shown to lower ROS levels in models of sepsis-induced cardiac injury.[42] Furthermore, NF-κB is known to promote IL-6, IL-8, and TNFα cytokine production, which play significant roles in the pathogenesis of ALI.[43,44] We found that treatment with CNP-miR146a at the time of injury is able to significantly reduce IL-6 gene expression three days following bleomycin injury. Furthermore, treatment with CNP-miR146a reduced IL-8 and TNFα gene expression seven days following injury. Preventing the early increase in IL-6, which is an early acute-phase reactant, may prevent an inflammatory cascade and prevent persistent elevation of IL-8 and TNFα at later time points (Figure 4).

Ultimately, the goal of treatment with CNP-miR146a is to improve long-term outcomes following ALI by decreasing fibrosis and improving pulmonary biomechanics, and long-term morbidity seen in ALI/ARDS is often driven by lung structural changes, such as interstitial fibrosis. CNP-miR146a lowers early TGFβ-1 signaling three days after injury and Col1α2 gene expression seven days following injury (Figures 4 and S2). This reduction in pro-fibrotic gene signaling correlated with reductions in collagen quantification on histologic analysis (Figure 5). While trichrome staining is a pan-collagen stain, the reduction in Col1α2 gene expression seen with CNP-miR146a treatment supports that the early reduction of inflammatory gene expression may result in a reduction of ROS production and pathologic remodeling.

The potential of CNP-miR146a in a clinical setting is highlighted by the prevention of pulmonary mechanical dysfunction with CNP-miR146a. While CNP alone and miR146a alone additionally lower ROS and inflammatory signaling, we found only the conjugate treatment to be effective in improving pulmonary mechanics (Figure 6). Treatment with CNP-miR146a at the time of injury improved pulmonary elastance, inspiratory capacity, pulmonary compliance, and tissue resistance. While CNP alone lowered inflammatory cell infiltrate and ROS levels, and miR146a alone lowered pro-inflammatory gene signaling, only the conjugate treatment improved pulmonary function. By lowering inflammatory

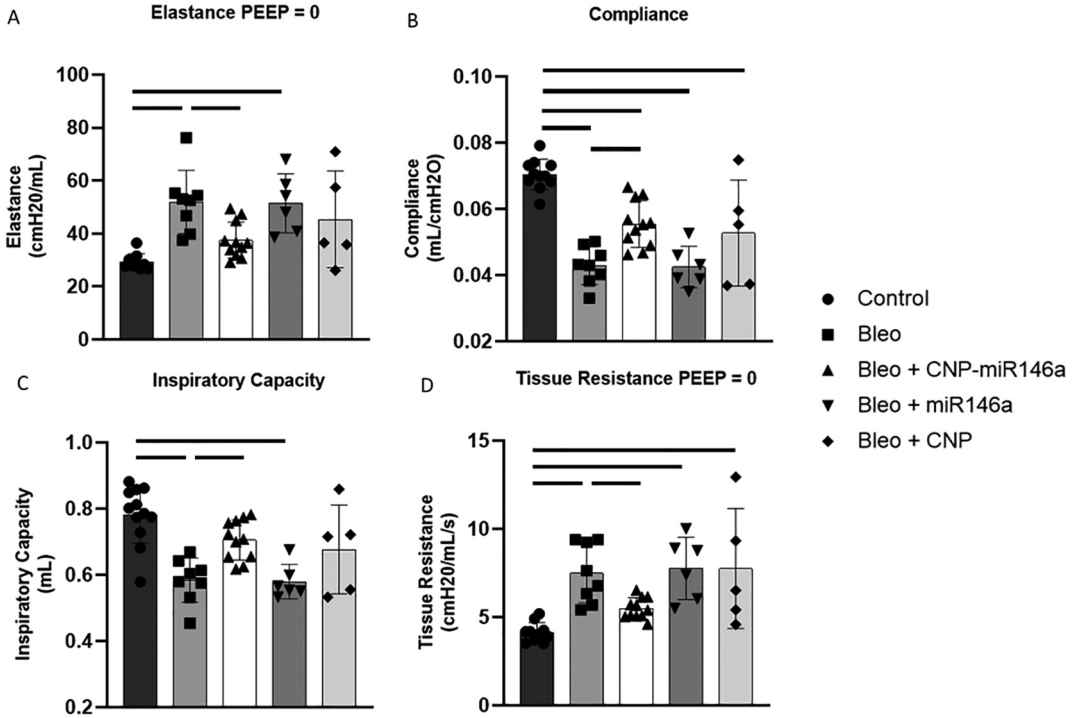

Figure 6. Pulmonary mechanics 14 days after bleomycin injury.Bleomycin-injured mice had significantly worse pulmonary compliance, tissue resistance, elastance, and inspiratory capacity compared to controls, while prevention treatment with CNP-miR146a improved pulmonary mechanics compared to untreated, bleomycin-injured lungs and returned function to control levels. Bars indicate statistical significance with $P < 0.05$. Mean and standard deviation for n = 12, 8, 6, 5, 11 for control, bleomycin, bleomycin + CNP, bleomycin + miR146a, bleomycin + CNP-miR146a samples are shown.

signaling and collagen deposition through the synergistic effects of CNP and miR146a, CNP-miR146a prevents acute lung injury and protects pulmonary function. This could prevent the need for mechanical ventilation or ICU admission, and prevent the need for long-term pulmonary rehabilitation.

Despite advances in mechanical ventilation and critical care, the progression of acute lung injury to ARDS results in devastating morbidity and an in-hospital mortality of nearly 40%.[45] There is a pressing need to develop novel therapeutics that may prevent ALI and protect pulmonary function. We have shown that utilization of nanotechnology with CNP to locally deliver miR146a can attenuate bleomycin-induced ALI by decreasing inflammation, oxidative stress, and resultant fibrosis, thereby protecting pulmonary function without systemic uptake.

Credit Author Statement

Stephen M. Niemiec: Conceptualization, data curation, formal analysis, investigation, methodology, project administration, visualization, roles/writing – original draft, writing – review & editing.

Sarah A. Hilton: Conceptualization, data curation, formal analysis, investigation, methodology, project administration, visualization, roles/writing – original draft, writing – review & editing.

Alison Wallbank: Data curation, investigation, methodology, project administration, writing – review & editing.

Mark Azeltine: Data curation, investigation, methodology, project administration, resources, writing – review & editing.

Amanda E. Louiselle: Data curation, investigation, methodology, project administration, writing – review & editing.

Hanan Elajaili: Data curation, investigation, methodology, project administration, writing – review & editing.

Ayed Allawzi: Data curation, investigation, methodology, project administration, writing – review & editing.

Junwang Xu: Conceptualization, resources, supervision, writing – review & editing.

Courtney Mattson: Data curation, investigation, methodology, project administration, writing – review & editing.

Lindel C. Dewberry: Data curation, investigation, methodology, project administration, writing – review & editing.

Junyi Hu: Data curation, investigation, methodology, project administration, resources, writing – review & editing.

Sushant Singh: Data curation, investigation, methodology, project administration, resources, writing – review & editing.

Tamil S Sakthivel: Data curation, investigation, methodology, project administration, resources, writing – review & editing.

Eva Nozik-Grayck: Conceptualization, funding acquisition, project administration, supervision, validation, writing – review & editing.

Bradford Smith: Conceptualization, funding acquisition, project administration, supervision, validation, writing – review & editing.

Sudipta Seal: Conceptualization, funding acquisition, project administration, supervision, validation, writing – review & editing.

Carlos Zgheib: Conceptualization, funding acquisition, project administration, supervision, validation, writing – review & editing.

Kenneth W. Liechty: Conceptualization, funding acquisition, project administration, supervision, validation, writing – review & editing.

Acknowledgments

The authors would like to thank the University of Colorado Denver Histology Shared Resource Center for their contribution to this work. This work was supported by a Gates Center Grubstake Award for the work presented in this publication.

Appendix A. Supplementary data

Supplementary data to this article can be found online at https://doi.org/10.1016/j.nano.2021.102388.

References

1. Katzenstein AL, Bloor CM, Leibow AA. Diffuse alveolar damage—the role of oxygen, shock, and related factors. A review. *Am J Pathol* 1976;**85**(1):209-28.
2. Piantadosi CA, Schwartz DA. The acute respiratory distress syndrome. *Ann Intern Med* 2004;**141**(6):460-70.
3. DiSilvio B, Young M, Gordon A, Malik K, Singh A, Cheema T. Complications and outcomes of acute respiratory distress syndrome. *Crit Care Nurs Q* 2019;**42**(4):349-61.
4. Pierrakos C, Karanikolas M, Scolletta S, Karamouzos V, Velissaris D. Acute respiratory distress syndrome: pathophysiology and therapeutic options. *J Clin Med Res* 2012;**4**(1):7-16.
5. Garbuzenko OB, Saad M, Betigeri S, Zhang M, Vetcher AA, Soldatenkov VA, et al. Intratracheal versus intravenous liposomal delivery of siRNA, antisense oligonucleotides and anticancer drug. *Pharm Res* 2009;**26**(2):382-94.
6. Gautam A, Waldrep CJ, Densmore CL. Delivery systems for pulmonary gene therapy. *Am J Respir Med* 2002;**1**(1):35-46.
7. Chen J, Patil S, Seal S, McGinnis JF. Rare earth nanoparticles prevent retinal degeneration induced by intracellular peroxides. *Nat Nanotechnol* 2006;**1**(2):142-50.
8. Dowding JM, Song W, Bossy K, Karakoti A, Kumar A, Kim A, et al. Cerium oxide nanoparticles protect against Abeta-induced mitochondrial fragmentation and neuronal cell death. *Cell Death Differ* 2014;**21**(10):1622-32.
9. Grulke E, Reed K, Beck M, Huang X, Cormack A, Seal S. Nanoceria: factors affecting its pro- and anti-oxidant properties. *Environ Sci-Nano* 2014;**1**(5):429-44.
10. Heckert EG, Karakoti AS, Seal S, Self WT. The role of cerium redox state in the SOD mimetic activity of nanoceria. *Biomaterials* 2008;**29**(18):2705-9.
11. Korsvik C, Patil S, Seal S, Self WT. Superoxide dismutase mimetic properties exhibited by vacancy engineered ceria nanoparticles. *Chem Commun (Camb)* 2007(10):1056-8.
12. Pirmohamed T, Dowding JM, Singh S, Wasserman B, Heckert E, Karakoti AS, et al. Nanoceria exhibit redox state-dependent catalase mimetic activity. *Chem Commun (Camb)* 2010;**46**(16):2736-8.
13. Sack M, Alili L, Karaman E, Das S, Gupta A, Seal S, et al. Combination of conventional chemotherapeutics with redox-active cerium oxide nanoparticles—a novel aspect in cancer therapy. *Mol Cancer Ther* 2014;**13**(7):1740-9.
14. Allawadhi P, Khurana A, Allwadhi S, Joshi K, Packirisamy G, Bharani KK. Nanoceria as a possible agent for the management of COVID-19. *Nano Today* 2020;**35**:100982.
15. Schwartz MD, Moore EE, Moore FA, Shenkar R, Moine P, Haenel JB, et al. Nuclear factor-kappa B is activated in alveolar macrophages from patients with acute respiratory distress syndrome. *Crit Care Med* 1996;**24**(8):1285-92.
16. Selvaraj V, Nepal N, Rogers S, Manne ND, Arvapalli R, Rice KM, et al. Inhibition of MAP kinase/NF-kB mediated signaling and attenuation of lipopolysaccharide induced severe sepsis by cerium oxide nanoparticles. *Biomaterials* 2015;**59**:160-71.
17. Kumari P, Saifi MA, Khurana A, Godugu C. Cardioprotective effects of nanoceria in a murine model of cardiac remodeling. *J Trace Elem Med Biol* 2018;**50**:198-208.
18. Fahy RJ, Lichtenberger F, McKeegan CB, Nuovo GJ, Marsh CB, Wewers MD. The acute respiratory distress syndrome: a role for transforming growth factor-beta 1. *Am J Respir Cell Mol Biol* 2003;**28**(4):499-503.
19. Dowdy SF. Overcoming cellular barriers for RNA therapeutics. *Nat Biotechnol* 2017;**35**(3):222-9.
20. Johannes L, Lucchino M. Current challenges in delivery and cytosolic translocation of therapeutic RNAs. *Nucleic Acid Ther* 2018;**28**(3):178-93.
21. Colon J, Hsieh N, Ferguson A, Kupelian P, Seal S, Jenkins DW, et al. Cerium oxide nanoparticles protect gastrointestinal epithelium from radiation-induced damage by reduction of reactive oxygen species and upregulation of superoxide dismutase 2. *Nanomedicine* 2010;**6**(5):698-705.
22. Hirst SM, Karakoti AS, Tyler RD, Sriranganathan N, Seal S, Reilly CM. Anti-inflammatory properties of cerium oxide nanoparticles. *Small* 2009;**5**(24):2848-56.
23. Karakoti A, Singh S, Dowding JM, Seal S, Self WT. Redox-active radical scavenging nanomaterials. *Chem Soc Rev* 2010;**39**(11):4422-32.
24. Walkey C, Das S, Seal S, Erlichman J, Heckman K, Ghibelli L, et al. Catalytic properties and biomedical applications of cerium oxide nanoparticles. *Environ Sci Nano* 2015;**2**(1):33-53.
25. Taganov KD, Boldin MP, Chang KJ, Baltimore D. NF-kappaB-dependent induction of microRNA miR-146, an inhibitor targeted to signaling proteins of innate immune responses. *Proc Natl Acad Sci U S A* 2006;**103**(33):12481-6.
26. Ghadiali SN, Bobba C, Ballinger MN, Englert JA. Nanoparticle-based delivery of microRNA-146a mitigates ventilator induced lung injury and inflammation. *Am J Resp Crit Care* 2019;**199**.
27. Mahida RY, Matsumoto S, Matthay MA. Extracellular vesicles: a new frontier for research in acute respiratory distress syndrome. *Am J Respir Cell Mol Biol* 2020;**63**(1):15-24.
28. Karakoti AS, Monteiro-Riviere NA, Aggarwal R, Davis JP, Narayan RJ, Self WT, et al. Nanoceria as antioxidant: synthesis and biomedical applications. *JOM (1989)* 2008;**60**(3):33-7.
29. Patil S, Kuiry SC, Seal S, Vanfleet R. Synthesis of nanocrystalline ceria particles for high temperature oxidation resistant coating. *J Nanopart Res* 2002;**4**(5):433-8.
30. Adamson IY, Bowden DH. The pathogenesis of bleomycin-induced pulmonary fibrosis in mice. *Am J Pathol* 1974;**77**(2):185-97.
31. Knudsen L, Lopez-Rodriguez E, Berndt L, Steffen L, Ruppert C, Bates JHT, et al. Alveolar micromechanics in bleomycin-induced lung injury. *Am J Respir Cell Mol Biol* 2018;**59**(6):757-69.
32. Matute-Bello G, Frevert CW, Martin TR. Animal models of acute lung injury. *Am J Phys Lung Cell Mol Phys* 2008;**295**(3):L379-99.
33. Elajaili HB, Hernandez-Lagunas L, Ranguelova K, Dikalov S, Nozik-Grayck E. Use of electron paramagnetic resonance in biological samples at ambient temperature and 77 K. *J Vis Exp* 2019;**143**.
34. Hantos Z, Daroczy B, Suki B, Nagy S, Fredberg JJ. Input impedance and peripheral inhomogeneity of dog lungs. *J Appl Physiol (1985)* 1992;**72**(1):168-78.
35. Niemiec SM, Louiselle AE, Hilton SA, Dewberry LC, Zhang L, Azeltine M, et al. Nanosilk increases the strength of diabetic skin and delivers CNP-miR146a to improve wound healing. *Front Immunol* 2020;**11**:590285.
36. De Marzi L, Monaco A, De Lapuente J, Ramos D, Borras M, Di Gioacchino M, et al. Cytotoxicity and genotoxicity of ceria nanoparticles on different cell lines in vitro. *Int J Mol Sci* 2013;**14**(2):3065-77.

37. Singh S, Ly A, Das S, Sakthivel TS, Barkam S, Seal S. Cerium oxide nanoparticles at the nano-bio interface: size-dependent cellular uptake. *Artif Cells Nanomed Biotechnol* 2018;**46**(sup3):S956-63.
38. Zgheib C, Hilton SA, Dewberry LC, Hodges MM, Ghatak S, Xu J, et al. Use of cerium oxide nanoparticles conjugated with microRNA-146a to correct the diabetic wound healing impairment. *J Am Coll Surg* 2019;**228**(1):107-15.
39. Fan EKY, Fan J. Regulation of alveolar macrophage death in acute lung inflammation. *Respir Res* 2018;**19**(1):50.
40. Tang L, Zhang H, Wang C, Li H, Zhang Q, Bai J. M2A and M2C macrophage subsets ameliorate inflammation and fibroproliferation in acute lung injury through interleukin 10 pathway. *Shock* 2017;**48**(1):119-29.
41. Thakur N, Manna P, Das J. Synthesis and biomedical applications of nanoceria, a redox active nanoparticle. *J Nanobiotechnol* 2019;**17**(1):84.
42. An R, Feng J, Xi C, Xu J, Sun L. miR-146a attenuates sepsis-induced myocardial dysfunction by suppressing IRAK1 and TRAF6 via targeting ErbB4 expression. *Oxid Med Cell Longev* 2018;**2018**:7163057.
43. Crimi E, Slutsky AS. Inflammation and the acute respiratory distress syndrome. *Best Pract Res Clin Anaesthesiol* 2004;**18**(3):477-92.
44. Kawano T, Mori S, Cybulsky M, Burger R, Ballin A, Cutz E, et al. Effect of granulocyte depletion in a ventilated surfactant-depleted lung. *J Appl Physiol (1985)* 1987;**62**(1):27-33.
45. Bellani G, Laffey JG, Pham T, Fan E, Brochard L, Esteban A, et al. Epidemiology, patterns of care, and mortality for patients with acute respiratory distress syndrome in intensive care units in 50 countries. *JAMA* 2016;**315**(8):788-800.